Transient Energy Protection based on Wavelet Packet Transform for Hybrid Bipolar HVDC Transmission System

Shuping Gao [1*], Xiaochen Song [1*], Huanfei Ye[2], Lin Jiang [3], Guobing Song [4]

[1] College of Electrical and Control Engineering, Xi'an University of Science and Technology, #58 Yanta Middle Road, Beilin District, Xi'an City, Shaanxi Province, China
[2] State Grid Shaanxi Electric Power Company Yulin Power Supply Company, Yulin, Shaanxi, China
[3] Department of Electrical Engineering & Electronics, University of Liverpool, L69 3GJ, Brownlow Hill, Liverpool, UK
[4] School of Electrical Engineering, Xi'an Jiaotong University, #28 Xianning West Road, Beilin District, Xi'an City, Shaanxi Province, China
1067704076@qq.com, 3453870983@qq.com, 1240980849@qq.com, ljiang@liv.ac.uk, song.gb@mail.xjtu.edu.cn

Abstract: In hybrid bipolar DC transmission systems with different types of converters at each pole, the transient high-frequency component of the voltage signal under a single-pole grounding fault and an inter-pole fault is significantly different for internal and external faults because of smooth-wave reactors on both sides of the DC line. Based on these characteristics, a single-ended electrical quantity protection scheme based on transient energy is proposed. First, the voltage fault component is extracted and then processed by using a wavelet packet transform to obtain the transient energy in each frequency band. Second, the protection criterion is determined based on the ratio between low-frequency energy and the sum of high-frequency energy. After the setting principle is given, the influence of the protection scheme under high transition resistance is analyzed. The protection scheme is implemented in MATLAB and tested based on fault data obtained from a hybrid bipolar HVDC transmission model built in PSCAD under different operating conditions. The effectiveness of the proposed protection method for hybrid bipolar HVDC transmission systems is verified by extensive simulation tests under different fault types in different fault distances. The proposed method can provide strong tolerance to high transient resistance, accurately identify internal/external faults and automatically identify fault poles.

1. Introduction

A high-voltage direct current (HVDC) transmission system has the advantages of low transmission loss and large transmission capacity [1], but it can suffer from commutation failure at the inverter end. A modular multilevel converter high-voltage direct current (MMC-HVDC) transmission system can provide independent control of active and reactive power without commutation failures and with reactive power support for faulty grids [2-3]. By combining the advantages of these two types of HVDC systems, four types of hybrid HVDC transmission systems with different topological structures have been proposed, which are hybrid two-terminal HVDC transmission systems, hybrid multi-terminal HVDC transmission systems, hybrid multi-infeed HVDC transmission systems and hybrid bipolar HVDC transmission systems[4-6].

This paper focuses on protecting a hybrid bipolar HVDC transmission system consisting of LCC-based positive poles and MMC-based negative poles. The MMC converter can provide fast reactive support capability and thus reduce the probability of LCC converter commutation failure on the inverter side. With the decreasing costs of power electronics, the economic benefit of this structure has improved. The topological structure of the system is especially suitable for grid interconnection projects with seasonal bidirectional power flow demands. At present, research on hybrid DC transmission systems has focused on the construction of system models and control modes, while there is little research on the protection of hybrid HVDC transmission lines[4-6]. DC transmission lines have a high failure rate because long transmission lines are easily affected by their operational environments. When a fault occurs, the fault should be identified accurately within a few milliseconds, which requires the reliable and rapid protection of the DC line [7]. Therefore, the safe and reliable operation of a hybrid HVDC transmission system requires a rapid protection scheme for the DC line.

There are two types of DC line protection schemes—double-end protection and single-end protection—that are categorized by the extracted electrical quantity of the converter station from either one end or both ends of the DC line [8-24]. Typical double-end protection in a conventional HVDC system utilizes pilot current differential protection as the backup protection, in which the compensation of the distributed capacitor current is not considered, so the protection action has a long delay[8]. Many new pilot protection schemes have been proposed [8-15]. However, because two-end protection requires the transmission of information on both sides of the line, those protection schemes cannot operate fast enough. Moreover, their performance can be degraded by insufficient communication channel reliability and data synchronicity. Unlike AC lines, DC lines have higher requirements for rapid protection and must respond quickly within a short time (a few milliseconds). Because two-end protection cannot meet the protection response time requirements, single-end protection without a communication channel is preferred [8-15].

The single-end protection used in most existing HVDC systems adopts travelling wave protection and

differential low-voltage protection as the main protection methods, which can respond quickly and only require data from one end. Single-end protection can distinguish both internal and external faults quickly without communication by using the information from one end of the DC line; however, they also have disadvantages such as poor resistance to high transition resistance and low sensitivity[16-24].In [16-17], the impedance characteristics of DC filtering links were analyzed to select the characteristic harmonic current and identify internal and external faults according to the fluctuation coefficient of the characteristic harmonic current. In [18-19], protection principles using the change rate of voltage measured at the line side of DC inductors were proposed. However, reliability under high-resistance faults could not be guaranteed. In addition, the required sampling frequency was much higher. In [20], a protection method based on the change rate of the DC inductor voltage was proposed. As the protection criterion only depended on the time required by the DC inductor voltage to change from one specific value to another, this method was easily affected by noise. In [21], a protection method using the high-frequency components of transient voltages on DC lines was proposed, providing fast operation speed and good robustness. However, an accurate theoretical basis was not analyzed thoroughly. In [22], a single-ended transient-voltage-based protection strategy was proposed, which has a higher reliability and stronger ability to endure high transition resistance, but the high transition resistance was only 300 Ω. In [23], a protection scheme based on the second-order difference of a backward voltage travelling wave was proposed. The high-resistance problem was overcome; however, the required time window exceeded 3 ms. In [24], a protection method using the transient high-frequency energy of the line current was proposed. Because the lumped parameter model was used as the DC line model, the propagation process of travelling waves on long transmission lines could not be reflected.

Wavelet transform is a new method of transform analysis, which overcomes the shortcoming of window size not changing with frequency. Its main feature is that it can fully highlight the characteristics of some aspects of the problem through transformation. Therefore, wavelet transform has been successfully applied in many fields, especially in power system protection[25-27]. However, there are still some shortcomings in wavelet transform. Since wavelet transform only decomposes the low-frequency sub-band in each stage of signal decomposition, the information of high-frequency sub-band cannot be extracted with the same high resolution.

Wavelet packet decomposition further optimizes the wavelet transform by compensating for the wavelet transform defects. Based on binary wavelet transform, wavelet packet transformation can realize the uniform division of signals. It can decompose the approximate coefficient and the detailed coefficient of the signals to better extract the time-frequency characteristics of the signals[28-30].

Based on the above analysis, this paper proposes a transient energy protection principle based on the wavelet packet transform for a hybrid bipolar DC transmission system to make full use of the advantages of wavelet packet transformation according to the differences in high- and low-frequency energies of the signal fault component when an internal or external fault occurs. First, the voltage fault component is extracted and processed by using the wavelet packet transform to obtain the transient energy level in each frequency band. Then, a protection criterion is constructed by using the ratio of low-frequency energy to the sum of partial high-frequency energy. A setting principle is given, and the influence of the transition resistance is analyzed. Finally, a hybrid bipolar HVDC transmission model is built in PSCAD to output the fault data, and the protection method is verified in MATLAB. Simulations under different operating conditions show that the protection method is suitable for hybrid bipolar HVDC transmission systems. Its data window is only 3 ms, and the method provides strong transient resistance. Internal or external faults can be identified accurately, and fault pole selection can be realized automatically.

The remainder of this paper is organized as follows. In Section 2, hybrid bipolar HVDC transmission systems are presented for fault characteristic analysis. In Section 3, fault characteristics for hybrid bipolar HVDC transmission lines are analyzed. In Section 4, the principle of boundary protection and the wavelet packet decomposition algorithm are outlined. In Section 5, the start-up criterion and the protection criterion are proposed, and the protection principle flow chart is presented. In Section 6, simulations are performed to evaluate the performance of the proposed protection method. Finally, conclusions are offered in Section 7.

2. Hybrid bipolar high-voltage transmission system structure and control method

2.1. Hybrid bipolar high-voltage transmission system structure

A ±500 kV hybrid HVDC transmission system is used to investigate the proposed protection scheme, and its topology is shown in Fig. 1. In Fig. 1, the positive pole adopts LCC-HVDC, whose converter unit is composed of a set of 12-pulse converters. The negative pole adopts MMC-HVDC, where each phase is formed by cascading 100 half-bridge modules. M and N are the two ends of the DC line, and a and c are the line protection installation positions, respectively; p and q are the positions used to install voltage dividers and current dividers on the positive and negative outlets in the rectifier side, respectively; Z is the AC side-equivalent impedance; L is a smoothing reactor; Table 1 lists the fault types and fault locations f_1 to f_7, which are shown in Fig. 1.

Table 1 Fault types and locations

Fault location	Fault type
f_1	External positive ground fault outside the rectifier side
f_2	Internal positive ground fault
f_3	Internal negative ground fault
f_4	External positive ground fault outside the inverter side
f_5	External negative ground fault outside the rectifier side
f_6	External negative ground fault outside the inverter side
f_7	Internal bipolar ground fault

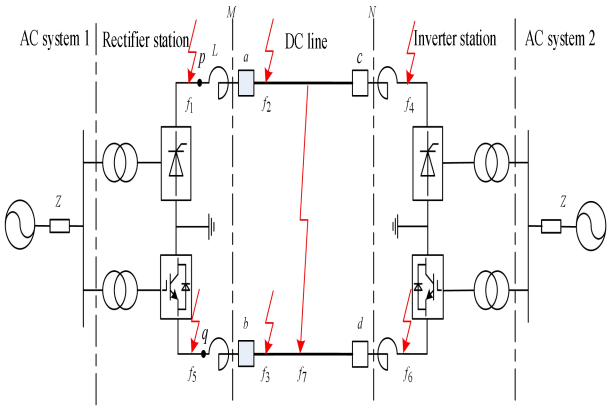

Fig. 1. *Hybrid bipolar DC transmission system*

2.2. Hybrid bipolar high-voltage transmission system control strategy

For the positive LCC-HVDC, constant DC current control is used on the rectification side, and trigger angle control and low-voltage current limit control are added. Constant DC current control and constant turn-off angle control are adopted on the inverter side, and a low-voltage current-limiting control is attached, as shown in Fig. 2.

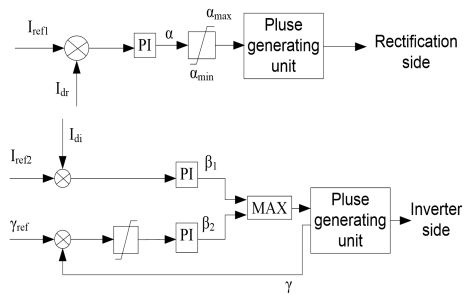

Fig. 2. *Diagram of the LCC control block*

For negative MMC-HVDC, the control methods include indirect current control and direct current control. Indirect current control controls the amplitude and phase of the AC side of the VSC converter and then regulates the power of the entire system. The control structure of this control method is simple, but it is greatly affected by system parameters. This paper uses the latter, which includes an outer loop voltage control and an inner loop current control. After decoupling, the current enters the trigger pulse generation circuit to generate pulse control signals, as shown in Fig. 3. Because the positive pole uses LCC-HVDC, commutation failure can occur on the inverter side. The control method of the negative pole MMC-HVDC can reduce the probability of positive phase commutation failure.

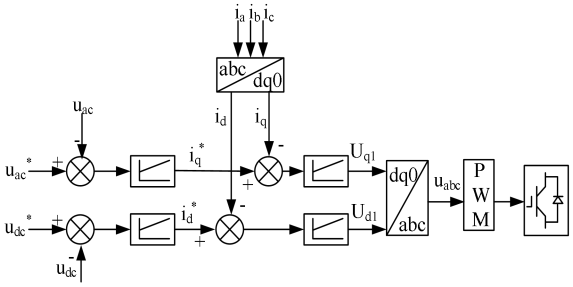

Fig. 3. *Diagram of MMC control block*

3. DC line fault characteristic analysis

Unipolar ground faults and bipolar short-circuit faults can occur on the DC side. When a unipolar ground fault occurs on the DC line of the system, the system can often maintain unipolar operation or operate at low voltage to ensure the transmission of active power. For DC lines, the control characteristics of the system will affect the fault characteristics. Differences in the topology and control strategies of different DC transmission systems will inevitably lead to differences in fault characteristics. The characteristic signal selected in this paper is the voltage signal, the fault occurrence time is 1 s, and the duration time is 0.1 s. When various faults occur, the fault waveforms measured at the protection measurement points are shown in Fig. 4.

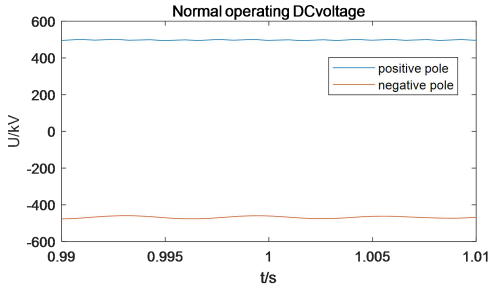

a

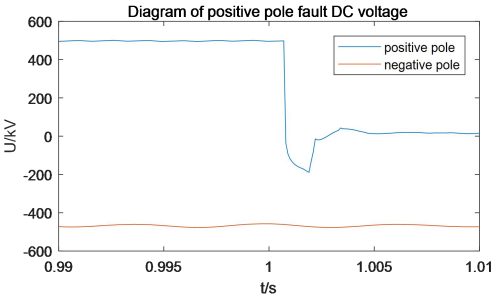

b

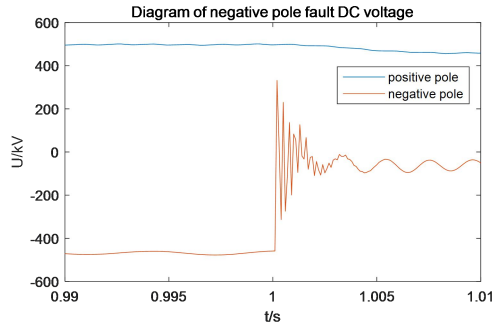

c

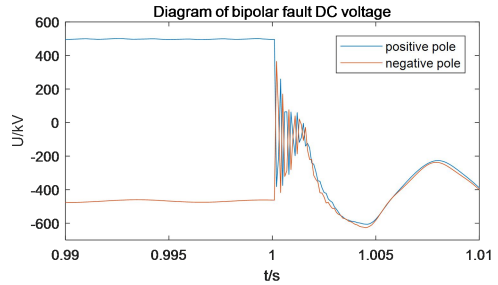

d

Fig. 4. *Waveforms of each fault in the hybrid bipolar DC line:* (a) *Normal operation voltage waveform,* ***(b)****Voltage waveform diagram when fault occurs on the positive pole,* ***(c)*** *Voltage waveform diagram when fault occurs on the negative pole,****(d)*** *Voltage waveform diagram during bipolar fault occurrence*

Fig. 4 shows that the voltage waveforms of the positive and negative faults are quite different, and the interpole fault characteristics are also different from those of the bipolar fault in single transmission mode. The transmission mode and control strategy adopted by the positive and negative poles affect the fault characteristics of the DC line. Due to the differences in unipolar fault characteristics, non-fault induction also differs from traditional single DC transmission methods. Therefore, it is necessary to study whether the transient energy ratio is still applicable to hybrid bipolar DC transmission systems. In other words, it is necessary to study not only whether the fault pole can operate correctly under these different fault characteristics but also whether the non-fault pole can operate reliably.

4. Protection principle and algorithm

4.1. Principle of boundary protection

The high-voltage hybrid bipolar DC transmission model built in this paper adopts a smoothing reactor as the protection boundary. The function of the smoothing reactor is to suppress the variations of current fault components when a fault occurs, prevent commutation failure and reduce harmonics. The larger the inductance value of the chosen DC reactor, the better the suppression effect on the high-frequency component is. However, if the value of the reactor is too large, it is easy to generate over-voltage during system operation, and the system control performance will worsen. Therefore, based on engineering experience, the value of smoothing reactor L is set as 0.01 H. The reason for its suppression effect on high-frequency components is reflected in (1) for calculating the impedance, which is:

$$Z = j\omega L \tag{1}$$

where ω is the angular frequency and L is the inductance value. Therefore, when L is constant, Z is proportional to ω, and the DC reactor has a significant suppression effect on high frequency.

4.1.1 Fault travelling wave when an internal fault occurs:

Taking the positive internal fault f_2 as an example. Fig. 5 shows a travelling wave diagram when an internal fault occurs at position f_2. When an internal fault occurs on the DC line, the travelling wave flows through both sides of the line from the fault point, refracts and reflects when it encounters an obstacle, and finally forms a loop through the ground.

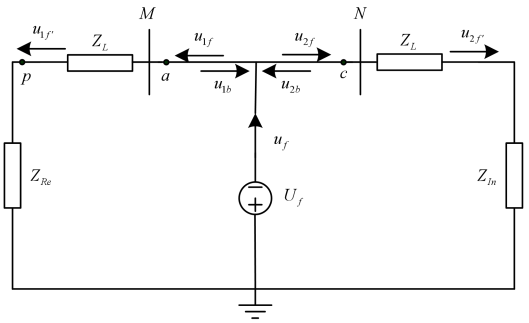

Fig. 5. *Fault travelling wave diagram when an internal fault occurs*

In Fig. 5, Z_L is the impedance of the line smoothing reactor. Assuming that the length from the fault point to position M is d, Z_{Re} and Z_{In} are the equivalent impedances of the converter on both sides. U_f is the additional network voltage source when a fault occurs. u_f is the travelling wave voltage generated when a fault occurs. It is divided into u_{1f} and u_{2f} when it flows through both sides of the line from the fault point. When encountering the smoothing reactor, the travelling wave is reflected and refracted on the line, which is divided into $u_{1f'}$, u_{1b} and $u_{2f'}$, u_{2b}. Thus, it can be seen that when an internal fault occurs on the positive DC line, the travelling wave encounters a flat-wave reactor during its propagation and energy attenuation occurs, namely:

$$E_a > E_p \tag{2}$$

where E_a and E_p represent the high-frequency transient energy of the travelling wave voltage at the a and p positions shown in Fig.1, respectively. Similarly, when an internal fault occurs in the negative DC line, at the negative pole on the rectifying side, there is:

$$E_b > E_q \tag{3}$$

where E_b and E_q represent the high-frequency transient energy of the travelling wave voltage at the b and q positions shown in Fig.1, respectively.

From the above analysis, it can be seen that when an internal fault occurs, the fault information contains rich high-

frequency and low-frequency information, and the travelling wave first flows through position *a* and position *c*, which are protection installation positions, and then flows through the smoothing reactor, which is called the boundary component. Due to the suppression effect of the smoothing reactor on the high-frequency energy, the fault current after passing through the smoothing reactor contains the majority of the low-frequency information, and the high-frequency energy is attenuated. The information obtained at measurement point *a* is the original high- and low-frequency information. Therefore, the high-frequency components obtained by the protection measuring device when an internal fault occurs are greater. Other internal faults are similar, and because the same conclusion can be drawn and space is limited, they will not be repeated in this paper.

4.1.2 Fault travelling wave when an external fault occurs at the rectifier side:

Taking the fault position f_1 shown in Fig.1 as an example, the fault travelling wave diagram is shown in Fig.6 when an external fault occurs.

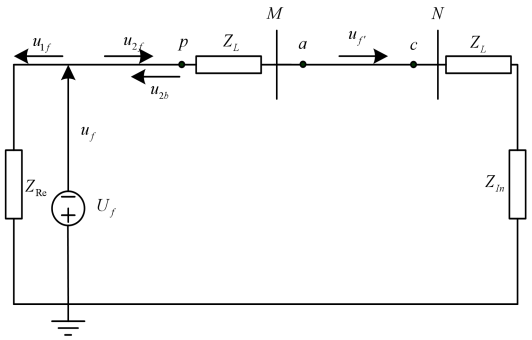

Fig. 6. *Fault travelling wave diagram when an external fault occurs outside the DC outlet of the rectifier side*

Fig. 6 shows that when the travelling wave propagates through the line, it flows through point *p* to the smoothing reactor, and refraction and reflection occur. This can be seen at the positive rectifier side in the relationship with the travelling wave transient energy between the voltage at *a* and *p*.

It can be seen that when an external fault occurs, the travelling wave propagation will attenuate through point *p* to the smoothing reactor. The transient energy relation between points *a* and *p* is as follows:

$$E_a < E_p \tag{4}$$

Similarly, when an external fault occurs outside the negative DC line, at the negative pole on the rectifying side, there is:

$$E_b < E_q \tag{5}$$

From the above analysis, when an external fault occurs, the travelling wave first flows through *p*, then passes through the smoothing reactor, and then reaches the protection installation. It can also be seen that there is less high-frequency information measured at the protection installation. Other external faults are similar, and the same conclusion can be drawn. Because space is limited, they will not be covered in this paper.

4.2. Wavelet packet transformation algorithm

In this paper, the high- and low-frequency transient energies at the boundary element are used for fault identification. Therefore, the high-frequency component of the signal needs to be decomposed. Since the wavelet transform only decomposes the low-frequency component of the signal, the wavelet function $\Psi_{ab}(t)$ is defined as:

$$\psi_{ab}(t) = |a|^{-\frac{1}{2}} \psi\left(\frac{t-b}{a}\right) \tag{6}$$

where *a* is called the scale parameter and *b* is called the position parameter.

The wavelet packet decomposition overcomes this defect by decomposing the approximation coefficient and detail coefficient of the signal.

For any scale *j*, the recursive expression of the function $\mu_{j,m}(t)$ is as follows:

$$\begin{cases} \mu_{j,2m}(t) = 2\sum_{n\in Z} h(n)\mu_{j-1,m}(2t-n) \\ \mu_{j,2m+1}(t) = 2\sum_{n\in Z} g(n)\mu_{j-1,m}(2t-n) \end{cases} \tag{7}$$

where the function $\mu_{j,m}(t)$ is called the wavelet packet of the wavelet function $\Psi_{ab}(t)$. $h(n)$ is the low-pass filter bank of the wavelet packet and $g(n)$ is the high-pass filter bank of the wavelet packet.

The wavelet packet transform expands the signal on the wavelet packet function system to obtain the inner product of the signal and the wavelet packet function. If the decomposition coefficient on scale *j* is $x_{j,m}(k)$, it can be expressed as:

$$x_{j,m}(k) = (f(t), 2^{-j/2}\mu_{j,m}(2^{-j}t-n)) \tag{8}$$

Thus, the recursive formula of wavelet packet decomposition is obtained as:

$$\begin{cases} x_{j,2m}(n) = \sqrt{2}\sum_{k\in Z} h(k-2n)x_{j-1,m}(k) \\ \mu_{j,2m+1}(t) = \sqrt{2}\sum_{n\in Z} g(k-2n)x_{j-1,m}(k) \end{cases} \tag{9}$$

where *j* represents the scale, *m* represents the frequency band, and *n* represents the time domain position of the point.

The energy obtained after the wavelet packet transform is defined as the integral of the transform coefficients at the scale along the time axis, so the energy of each frequency band decomposed by the i^{th} wavelet packet can be expressed as:

$$E_i = \sum_{k=1}^{N} \left|W(i,j)\right|^2 \tag{10}$$

In (10), E_i refers to the i^{th} transform energy, *W(i, j)* is the wavelet packet coefficient after the wavelet packet decomposition, and *N* is the number of samples.

4.3. Wavelet packet transformation parameters

In this paper, the sampling period is 100 μs, and the sampling frequency is 10 kHz. In practical engineering, useful fault information can be extracted when the sampling frequency exceeds 2 kHz. The nodes in the third layer are distributed from small to large according to the frequency. According to the Nyquist sampling law, the highest frequency is 5 kHz, which is divided into 8 nodes, and the number of diagram of wavelet packet decomposition is shown in Fig.7. The frequency segment distribution of each node is shown in Table 2.

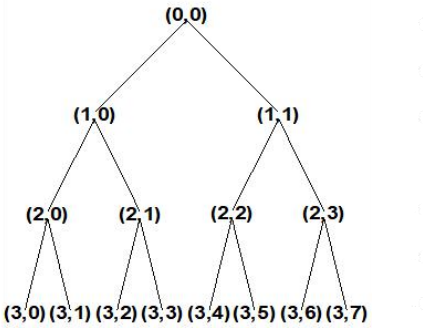

Fig.7. *The number of diagram of wavelet packet decomposition*

Table 2 Wavelet packet decomposition frequency segment corresponding to each node of layer 3

Node	Frequency range (Hz)	Node	Frequency range (Hz)
1	0-625	5	2500-3125
2	625-1250	6	3125-3750
3	1250-1875	7	3750-4375
4	1875-2500	8	4375-5000

In Table 2, it can be seen that the frequency range of node 1 includes the fundamental wave frequency. Because the long lines have a certain enhancement effect on the low-frequency signal, the frequency energy level of node 1 is very large, which can also be verified in the subsequent simulation.

As the order of magnitude of the energy value of node 1 is too large, which is very different from the order of magnitude of the subsequent node, the data of node 1 are removed in fault identification. In order to facilitate the analysis, the node 2 data are used as a low-frequency band energy and the sum of the data from node 3 to node 6 is used as the high-frequency band energy.The ratio of high-frequency energy to low-frequency energy of the voltage is used to constitute the protection criterion.

5. Single-ended electrical quantity protection based on energy distribution

In this paper, a single-ended electric quantity protection principle is presented, which is based on the ratio of transient energy of boundary elements by using the smoothing reactor inherent on both sides of the hybrid bipolar direct current transmission lines. By performing wavelet packet transform on the voltage fault component extracted from the position of the protection device installed when a fault occurs, the wavelet packet decomposition coefficients of each node are obtained, and the transient energy of each frequency band is obtained by (10).

Since the inductance has the characteristics of passing through a low-frequency signal and resisting a high-frequency signal, the protection criterion is constructed by using the ratio of the low-frequency energy to the sum of partial high-frequency energy. According to the protection criterion, internal or external faults can be identified, and fault pole selection can be implemented.

5.1. Protection starting criterion

In this paper, the protection starting criterion can be constructed according to the magnitude of the voltage fault component after a fault occurs, which can be expressed as:

$$\left|\Delta U\right| > 0.1U_n \tag{11}$$

In (11), ΔU is the positive or negative voltage fault component after a fault occurs, which is calculated from the instantaneous voltage value minus its value 1 ms ago. U_n is the rated voltage, which is 500 kV in this paper. If the value of the voltage fault component meets (11), the protection device engages. Otherwise, the protection device does not engage.

5.2. Protection criteria

According to the above analysis, the high-frequency energy of the voltage obtained from the measuring point of protection is large when an internal fault occurs, and the high-frequency energy of the voltage obtained from the measurement point is small when an external fault occurs. Therefore, the ratio of high-frequency energy to low-frequency energy of the voltage is also different when an internal or external fault occurs. According to this feature, a protection criterion can be constructed as follows:

$$\begin{cases} K_a = E_{La} / E_{\Sigma Ha} < K_{set} \\ K_b = E_{Lb} / E_{\Sigma Hb} < K_{set} \end{cases} \tag{12}$$

In (12), K_a and K_b represent the ratio of the low-frequency energy of the voltage fault component to the high-frequency energy of the voltage fault component in the positive and negative poles, respectively; E_{La} is the second node's energy value for the voltage fault component after being transformed by the wavelet packet for three layers; $E_{\Sigma Ha}$ is the sum of the energy of the later six nodes of the third layer after being transformed by the wavelet packet for three layers. K_{set} is the threshold value.

For the selection of the threshold value, it is only necessary to ensure that it can avoid all the external faults. From a large number of simulation data, it can be found that there exists a significant difference between the energy ratios when an internal or external fault occurs. Therefore, considering a certain margin value, the threshold value of K_{set} can be selected as:

$$K_{set} = 3 \tag{13}$$

Therefore, the protection criteria can be set as follows:

The protection criteria of the internal positive pole fault are K_a<3 and K_b>3.

The protection criteria of the internal negative pole fault are K_a>3 and K_b<3.

The protection criteria of the internal bipolar fault are K_a<3 and K_b<3.

The protection criteria of the external fault are K_a>3 and K_b>3.

According to the protection criteria, internal or external faults can be identified. At the same time, if the fault is an internal fault, it can be seen that the protection criteria can also achieve the fault pole selection solely from the above results, and the fault pole or the non-fault pole can also be identified accurately.

5.3. Protection flow chart

The protection flow chart is shown in Fig. 8. From Fig. 8, the first step is to determine whether a fault has occurred and whether the protection device has engaged. If so, the wavelet packet transform is implemented on the voltage fault component, and the energy of each node is obtained. Then, by calculating the ratio of low-frequency energy to high-frequency energy of the voltage fault component, according to the protection criteria, internal or external faults can be identified, and fault pole selection can be implemented.

In addition, because the data window of lightning strikes is microseconds and the data window of the protection method proposed in this paper is milliseconds, theoretically, this protection method is not affected by lightning strikes. In addition, the impact of lightning strikes will be specifically studied.

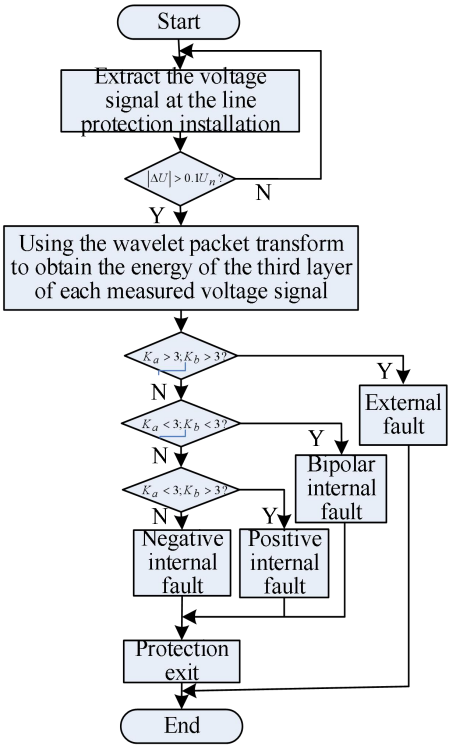

Fig. 8. *Protection flow chart*

6. Simulation verification

The cable length selected in the hybrid bipolar DC transmission system is 200 km and its line model is frequency dependent (phase) model shown in Fig. 9. Coaxial Cable is taken in simulation. The cable is a central solid conductor and may have up to three concentric conductors around the centre, each of which is separated by an insulator and its parameters is shown in Fig.10.

In simulation, the fault occurrence time is 3 s, and its duration time is 0.1 s. The data window selected is 3 ms, the sampling time is 100 μs, and the sampling frequency is 10 kHz.

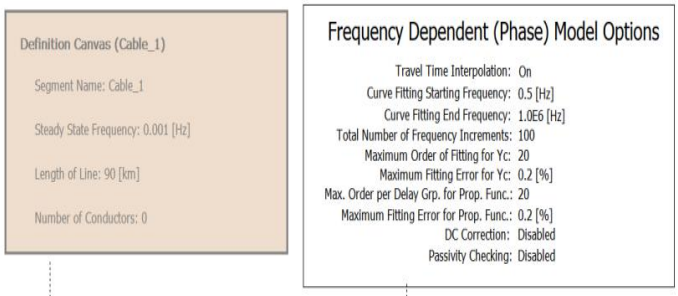

Fig. 9. *Frequency dependent (phase) model parameters*

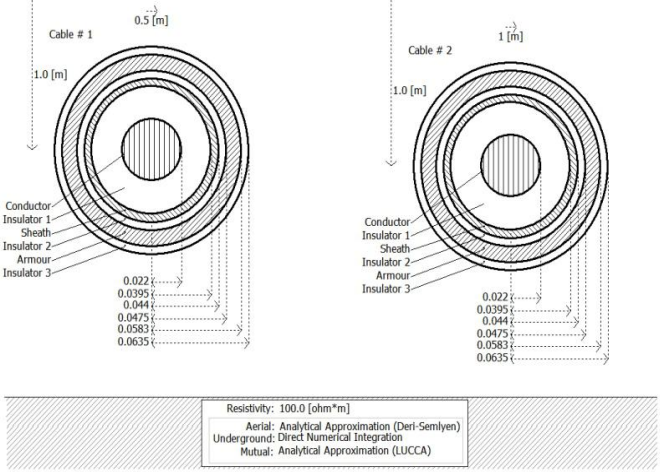

Fig. 10. *Coaxial cable parameters*

6.1. Simulation results when an internal fault occurs

When an internal fault occurs, according to the voltage data measured at positions *a* and *b* where the line protection device is installed, the voltage fault components can be calculated. Then, the transient high-frequency energy of the voltage fault component can be obtained by using the wavelet packet transform. In the end, the ratio of the energy of the second node to the sum of the energy of the later six nodes can be calculated. Comparing the ratio values with the threshold value of K_{set} according to the protection criteria, internal or external faults can be identified, and fault pole selection can be implemented.

6.1.1 Simulation results when a fault occurs in the positive line of hybrid bipolar DC transmission system:

When a fault occurs in the positive line of hybrid bipolar DC transmission system, the values of K_a and K_b are shown in Table 3, which are obtained in the cases of different single-pole grounding fault with different transition resistances in different fault distance from the rectifier converter station in a positive line. In Table 3, the value of $\frac{K_a}{K_b}$ means that the numerator is K_a and the denominator is K_b.

Table 3 The values of $\frac{K_a}{K_b}$ when an internal fault occurs in the positive line

$\frac{K_a}{K_b}$ Distance (km) / Transition resistance (Ω)	5	20	60	100	140	180	195
0.01	0.67	0.49	1.56	0.99	1.88	1.67	0.38
	5.49	6.52	3.62	5.06	4.95	4.73	4.64
100	1.39	1.45	1.22	1.60	1.63	1.09	0.81
	4.17	5.00	4.82	5.57	6.32	5.83	3.94
300	1.52	1.59	1.33	1.33	1.45	1.88	1.23
	3.86	4.26	4.58	3.61	7.37	5.92	4.33
500	1.60	1.72	1.56	1.09	1.38	2.71	1.66
	4.31	4.04	4.23	3.61	7.49	5.78	4.35
1000	1.81	2.04	2.44	1.06	1.63	2.86	2.87
	3.94	3.66	4.83	3.49	7.29	5.81	4.31

According to Table 3, *K*-value diagram of different transition resistances in different fault distance in positive internal faults is shown in Fig. 11.

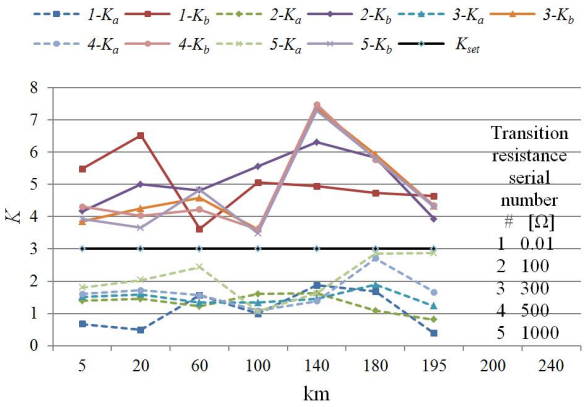

Fig. 11. *K-value diagram of different transition resistances with different distance when a positive internal fault occurs*

In Fig. 11, Fig.12 and Fig. 13, the horizontal axis represent the fault distance from the rectifier converter station to the fault position . The vertical axis is the value of *K*, which represents K_a, K_b and K_{set}. K_a and K_b are the values of different fault conditions in different distance. *1*-K_a and *1*-K_b are the value of K_a and K_b with 0.01 Ω transition resistance, respectively. *2*-K_a and *2*-K_b are the value of K_a and K_b with 100 Ω transition resistance, respectively. *3*-K_a and *3*-K_b are the value of K_a and K_b with 300 Ω transition resistance, respectively. *4*-K_a and *4*-K_b are the value of K_a and K_b with 500 Ω transition resistance, respectively. *5*-K_a and *5*-K_b are the value of K_a and K_b with 1000 Ω transition resistance, respectively.

In Fig. 11, it is clearly seen that all the values of K_a at position *a* where line protection is installed are less than 3, and all the values of K_b at position *b* where line protection is installed are greater than 3. Combined with the protection criteria, it indicates that an internal fault occurs on the positive line.

6.1.2 Simulation results when a fault occurs in the negative line of hybrid bipolar DC transmission system:

When a fault occurs in the negative line of hybrid bipolar DC transmission system, the values of K_a and K_b are shown in Table 4, which are obtained in the cases of different single-pole grounding fault with different transition resistances in different fault distance from the rectifier converter station in a negative line. In Table 4, the value of $\frac{K_a}{K_b}$ means that the numerator is K_a and the denominator is K_b.

Table 4 The values of $\frac{K_a}{K_b}$ when an internal fault occurs on the negative line

$\frac{K_a}{K_b}$ Distance (km) / Transition resistance (Ω)	5	20	60	100	140	180	195
0.01	5.49	5.59	5.07	4.39	5.26	5.52	5.67
	0.67	0.44	2.87	0.89	1.91	2.82	0.80
100	6.50	6.25	6.13	6.47	6.49	5.68	5.39
	1.23	1.32	1.55	0.83	1.35	1.95	0.52
300	6.59	6.40	6.22	6.57	6.74	6.26	6.07
	1.34	1.47	1.65	0.67	1.25	1.92	0.49
500	6.62	6.41	6.25	6.60	6.78	6.37	6.21
	1.37	1.56	1.77	0.55	1.17	2.28	0.44
1000	6.62	6.43	6.29	6.63	6.82	6.49	6.32
	1.50	1.79	2.03	0.56	0.90	2.72	0.53

According to Table 4, *K*-value diagram of different transition resistances in different fault distance in a negative internal faults is shown in Fig. 12.

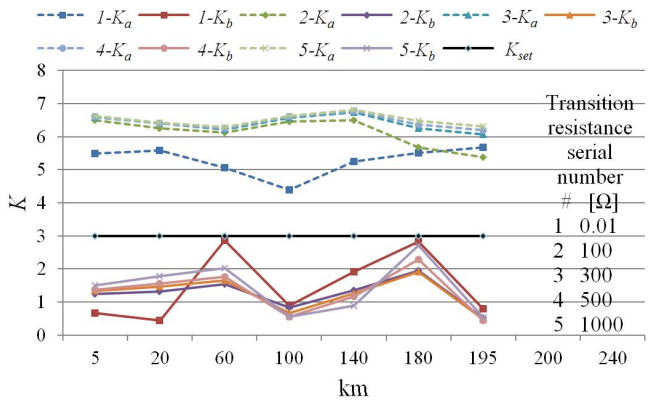

Fig. 12. *K-value diagram of different transition resistances with different distance when a negative internal fault occurs*

In Fig. 12, the simulation results show that all the values of K_a at position *a* where line protection is installed are greater than 3, and all the values of K_b at position *b* where line protection is installed are less than 3. Combined with the protection criteria, it can be verified that a negative internal fault occurs.

6.1.3 Simulation results when a bipolar fault occurs in the positive and negative line of hybrid bipolar DC transmission system:

When a bipolar fault occurs in the positive and negative line of hybrid bipolar DC transmission system at the same time, the values of K_a and K_b are shown in Table 5, which are obtained in the cases of different grounding fault with different transition resistances in different fault distance from the rectifier converter station to the fault location. In Table 5, the value of $\frac{K_a}{K_b}$ means that the numerator is K_a and the denominator is K_b.

Table 5 The values of $\frac{K_a}{K_b}$ when an internal fault occurs in the positive and negative line at the same time

$\frac{K_a}{K_b}$ Distance (km) / Transition resistance (Ω)	5	20	60	100	140	180	195
0.01	0.71 0.62	0.48 0.46	1.77 2.64	1.09 0.78	1.99 2.43	1.07 2.85	0.69 0.85
100	1.30 1.13	1.30 1.21	1.22 1.57	1.63 0.83	1.75 1.48	0.90 2.06	0.81 0.56
300	1.45 1.25	1.50 1.39	1.25 1.59	1.55 0.89	1.63 1.36	1.35 2.01	1.00 0.56
500	1.50 1.30	1.56 1.46	1.29 1.66	1.39 0.85	1.54 1.39	1.75 2.21	1.18 0.52
1000	1.60 1.36	1.73 1.58	1.56 1.84	1.06 0.83	1.46 1.22	2.79 2.17	1.70 0.47

According to Table 5, *K*-value diagram of different transition resistances in different fault distance when a bipolar internal fault occurs is shown in Fig. 13.

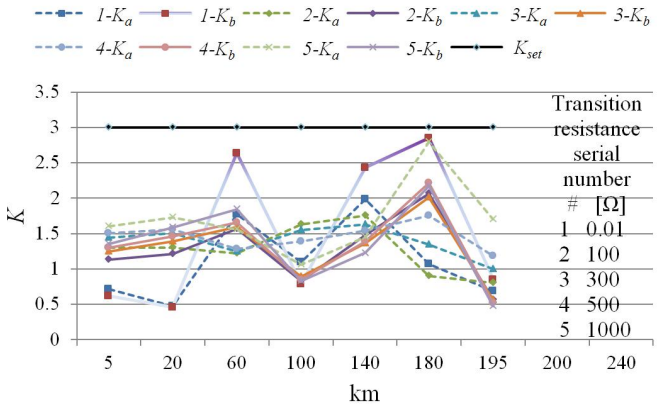

Fig. 13. *K-value diagram of different transition resistances with different distance when a bipolar internal fault occurs*

In Fig. 13, the simulation results show that all the values of K_a at position *a* where line protection is installed are less than 3, and all the values of K_b at position *b* where line protection is installed are less than 3. Combined with the protection criteria, it can be verified that a bipolar internal fault occurs.

6.2. Simulation results when an external fault occurs

The protection criterion is set to avoid the most serious external faults. When an external metal grounding fault occurs, the value of the protection setting is closest to the internal high-resistance grounding fault. Thus, if the protection device can successfully avoid the external metal grounding fault, it can be guaranteed to avoid all other external faults. In this paper, when an external fault with a grounding resistance of 0.01 Ω occurs, the values of K_a and K_b are shown in Table 6, where the value of $\frac{K_a}{K_b}$ means that the numerator is K_a and the denominator is K_b.

Table 6 Different values of $\frac{K_a}{K_b}$ when an external fault occurs

Transition Resistance (Ω)	f_1	f_4 (Fig. 13)	f_5	f_6
0.01	5.31 4.76	10.94 3.86	13.89 5.15	17.06 9.30

According to Table 6, *K*-value diagram for different external fault types is shown in Fig.14.

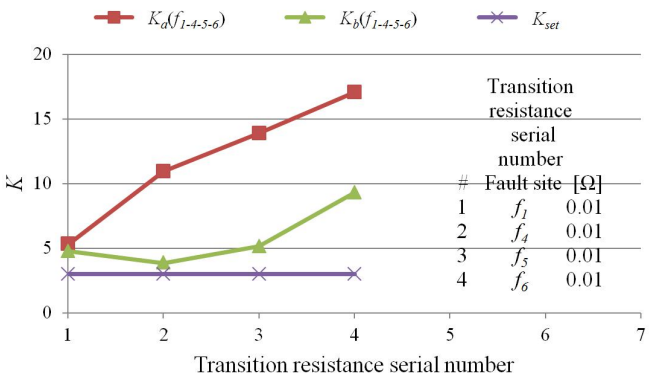

Fig. 14. *K-value diagram for different external fault types*

In Fig. 14, the horizontal axis transition resistance serial numbers 1, 2, 3 and 4 represent the external faults located at positions f_1, f_4, f_5 and f_6 shown in Fig. 1, and the vertical axis represents the values of K_a and K_b when an external fault occurs. The names corresponding to each line are $K_a(f_{1\text{-}4\text{-}5\text{-}6})$, $K_b(f_{1\text{-}4\text{-}5\text{-}6})$ and K_{set}. It can be seen that all the values *of* K_a at position *a* where line protection is installed are greater than 3, and all the values of K_b at position *b* where line protection is installed are greater than 3. Combined with the protection criteria, it can be verified that f_1, f_4, f_5 and f_6 are external faults.

6.3. Fault pole selection

For a bipolar DC transmission system, when an internal fault occurs on one pole, the other pole will also be affected.

When a single-pole fault occurs, the line protection at the fault pole starts, and the protection component operates. Then, the fault pole is isolated, and the DC system achieves single-pole operation. When a bipolar fault occurs, the protection engages, and the system cannot continue to work. Therefore, the most serious fault of internal faults is the bipolar fault. Table 7 shows the fault pole selection results.

Table 7 Fault pole selection results

Condition K_a	Condition K_b	Fault type	Identify result	Protection exit
<3	>3	f_2	Positive fault in the line	*a, c* operate
>3	<3	f_3	Negative pole fault in the line	*b, d* operate
<3	<3	f_7	Bipolar fault in the line	*a, b, c, d* operate

As seen in Table 7, fault pole selection can be implemented correctly.

To sum up, a lot of simulation results show that the protection method proposed in this paper can distinguish the internal and external faults accurately and rapidly. Moreover, it can operate to the internal fault in 3ms with high reliability. Even in the case of high resistance fault with 1000Ω transition resistance, the proposed protection method can still recognize the fault accurately and quickly. Therefore, compared with the traditional travelling wave protection, the protection method has a strong ability of bearing the high transition resistance. In addition, it has the ability to select poles automatically.

7. Conclusion

In this paper, by using the unique boundary structure of a hybrid bipolar DC transmission system, a DC line fault identification method is presented, which is based on the ratio of low-frequency energy to high-frequency energy in the transient voltage component when an internal or external fault occurs. The hybrid bipolar high-voltage direct current transmission system is built in PSCAD to simulate the different fault conditions. The protection method is implemented in MATLAB. The simulation results are as follows:

(1) Under different conditions, even in the case of an internal fault with 1000 Ω grounding resistance, the protection principle can still identify the fault accurately and rapidly, which satisfies the reliability of relay protection.

(2) The data window is only 3 ms and the protection method can operate in 3ms to the internal fault, which satisfies the rapidity of relay protection.

(3) The protection principle can protect the full length of the DC line, which satisfies the sensitivity of relay protection.

(4) The protection principle can quickly identify faults and perform fault pole selection by itself, which can meet the selectivity of relay protection.

(5) Wavelet packet decomposition is a more detailed decomposition method than wavelet decomposition. It provides a new method for fault identification of power system. Considering the computational amount of this protection method based on the wavelet packet transform, which may become the computational burden of low performance CPU, it is suggested that wavelet packet related computation can be implemented by hardware such as FPGA or CPLD to ensure that the protection principle can quickly and accurately identify the fault, and has high reliability.

In summary, the protection principle has a strong ability to endure high fault resistance and can meet the reliability, selectivity, rapidity and sensitivity of relay protection. The protection principle has high accuracy and the fault pole can be identified accurately.

8. Acknowledgment

The authors gratefully acknowledge the support of the National Natural Science Foundation of China (No.51777166) and National Natural Science Foundation Joint Fund Support Project (U1766209).And this research is supported by China Scholarship Council Fund.

9. References

[1]Xiao, H., Li, Y., Liu, R., et al.: 'Single-end time-domain transient electrical signals based protection principle and its efficient setting calculation method for LCC-HVDC lines',

IET Generation, Transmission & Distribution, 2017, 11, (5), pp. 1233-1242
[2]Wang, Z., Zhang, A., Zhang, H., et al.: 'Control Strategy for Modular Multilevel Converters With Redundant Sub-modules Using Energy Reallocation', IEEE Transactions on Power Delivery, 2017, 32, (3), pp. 1556-1564
[3]Yang, H., Li, W., Lin, L., et al.: 'Decoupled Current Control with Synchronous Frequency Damping for MMC Considering Sub-module Capacitor Voltage Ripple', IEEE Transactions on Power Delivery, 2018, 33, (1), pp. 419-428
[4]Zhang, Z., Xu, Z., Xue, Y., et al.: 'DC-Side Harmonic Currents Calculation and DC-Loop Resonance Analysis for an LCC–MMC Hybrid HVDC Transmission System', IEEE Transactions on Power Delivery, 2015, 30, (2), pp. 642-651
[5]Tang, G., Xu. Z.: 'A LCC and MMC hybrid HVDC topology with DC line fault clearance capability', International Journal of Electrical Power and Energy Systems, 2014, 62, pp. 419-428
[6]Haleem, N. M., Rajapakse, A. D., Gole, A. M., et al.: 'Investigation of Fault Ride-Through Capability of Hybrid VSC-LCC Multi-Terminal HVDC Transmission Systems', IEEE Transactions on Power Delivery, 2019, 34, (1), pp. 241-250
[7]Zheng, X., Tai, N., Wu, Z., et al.:'Harmonic current protection scheme for voltage source converter-based high-voltage direct current transmission system', IET Generation, Transmission & Distribution, 2014, 8, (9), pp. 1509-1515
[8]Zheng, J., Wen, M., Chen, Y., Shao, X.: 'A novel differential protection scheme for HVDC transmission lines'. International Journal of Electrical Power and Energy Systems, 2018, 94, pp. 171-178
[9]Takeda, H., Ayakawa, H., Tsumenaga, M., Sanpei, M.: 'New protection method for HVDC lines including cables', IEEE Transactions on Power Delivery, 1995, 10, (4), pp. 2035-2039
[10]Gao, S., Song, G., Ma, Z., et al.: 'Novel pilot protection principle for high-voltage direct current transmission lines based on fault component current characteristics', IET Generation, Transmission & Distribution, 2015, 9, (5), pp. 468-474
[11]Luo, S., Dong, X., Shi, S., et al.: 'A directional protection scheme for HVDC transmission lines based on reactive energy', IEEE Transactions on Power Delivery, 2016, 31, (2), pp. 559-567
[12]Gao, S., Liu, Q., Song, G.: 'Current differential protection principle of HVDC transmission system', IET Generation, Transmission & Distribution, 2017, 11, (5), pp. 1286-1292
[13]Kong, F., Hao, Z., Zhang, B.: 'Improved differential current protection scheme for CSC-HVDC transmission lines', IET Generation, Transmission & Distribution, 2017, 11, (4), pp. 978-986
[14]Li, Y., Zhang, Y., Song, J., Zeng, L., Zhang, J.: 'A novel pilot protection scheme for LCC-HVDC transmission lines based on smoothing-reactor voltage', Electric Power Systems Research, 2019, 168, pp. 261-268
[15]Zheng, J., Wen, M., Qin, Y., Wang, X., Bai, Y.: 'A novel pilot directional backup protection scheme based on transient currents for HVDC lines', International Journal of Electrical Power and Energy Systems, 2020, 115, pp. 1-9
[16]Song, G., Chu, X., Gao, S., et al.: 'A New Whole-Line Quick-Action Protection Principle for HVDC Transmission Lines Using One-End Current', IEEE Transactions on Power Delivery, 2015, 30, (2), pp. 599-607
[17]Liu, J., Tai, N., Fan, C., Huang, W.: 'Protection scheme for high-voltage direct-current transmission lines based on transient AC current', IET Generation, Transmission & Distribution, 2015, 9, (16), pp. 2633-2643
[18]Sneath, J., Rajapakse, AD.: 'Fault Detection and Interruption in an Earthed HVDC Grid Using ROCOV and Hybrid DC Breakers', IEEE Transactions on Power Delivery, 2016, 31, (3), pp. 971-981
[19]Leterme, W., Beerten, J., Van Hertem, D.: 'Nonunit Protection of HVDC Grids With Inductive DC Cable Termination', IEEE Transactions on Power Delivery, 2016, 31, (2), pp. 820-828
[20]Li, R., Xu, L., Yao, L.: 'DC Fault Detection and Location in Meshed Multiterminal HVDC Systems Based on DC Reactor Voltage Change Rate', IEEE Transactions on Power Delivery, 2017, 32, (3), pp. 1516-1526
[21]Xiang, W., Yang, S., Xu, L., et al.: 'A transient voltage-based DC fault line protection scheme for MMC-based DC grid embedding DC breakers', IEEE Transactions on Power Delivery, 2019, 34, (1), pp. 334-345
[22]Li, B., Li, Y., He, J., Wen, W.: 'A Novel Single-Ended Transient-Voltage-Based Protection Strategy for Flexible DC Grid', IEEE Transactions on Power Delivery, 2019, 34, (5), pp. 1925-1937
[23]Kong, F., Hao, Z., Zhang, B.: 'A Novel Traveling-Wave-Based Main Protection Scheme for ±800 kV UHVDC Bipolar Transmission Lines', IEEE Transactions on Power Delivery, 2016, 31, (5), pp. 2159-2168
[24]Li, Y., Wu, L., Li, J., Xiong, L., et al.:'DC Fault Detection in MTDC Systems Based on Transient High Frequency of Current', IEEE Transactions on Power Delivery, 2019, 34, (3), pp. 950-962
[25]Xiang, L., Zhi, B., Pei, L., et al.: 'A Wavelet Transform Based Non-communication Protection Technique for EHV Transmission Lines', Hkie Transactions, 2003, 10, (2), pp. 49-54
[26]Eldin, E.:'A Wavelet Technique for Directional Protection for EHV Transmission Lines with Series Compensation', International Journal of Power and Energy Systems, 2005, 25, (2), pp. 135-139
[27]Kerf, K. D., Srivastava, K., Reza, M., et al.: 'Wavelet-based protection strategy for DC faults in multi-terminal VSC HVDC systems', IET Generation,Transmission & Distribution, 2011, 5, (4), pp. 496-503
[28]Saleh, S. A., Rahman, M. A.: 'Modeling and protection of a three-phase power transformer using wavelet packet transform', IEEE Transactions on Power Delivery, 2005, 20, (2), pp. 1273-1282

[29]Zhang, Z., Wang, Y., Wang, K.: 'Fault diagnosis and prognosis using wavelet packet decomposition, Fourier transform and artificial neural network', Journal of Intelligent Manufacturing, 2013, 24, (6), pp. 1213-1227
[30]Alves, D., Costa, F. B., Lucio, D., et al.: 'Real-time power measurement using the maximal overlap discrete wavelet-packet transform',IEEE Transactions on Industrial Electronics, 2017, 64, (4), pp. 3177-3187